Monthly Notices of the ROYAL ASTRONOMICAL SOCIETY

MNRAS **530,** 1414–1423 (2024) https://doi.org/10.1093/mnras/stae727
Advance Access publication 2024 March 12

Seeing and turbulence profile simulations over complex terrain at the Thai National Observatory using a chemistry-coupled regional forecasting model

Ronald Macatangay,[1]★ Somsawatt Rattanasoon,[1] Timothy Butterley ,[2]★ Sherin Hassan Bran,[1] Thiranan Sonkaew,[3]★ Boonchoo Sukaum,[1] Donrudee Sookjai,[3] Mana Panya[1] and Titaporn Supasri[1]

[1]*National Astronomical Research Institute of Thailand, Don Kaeo, Mae Rim District, Chiang Mai 50180, Thailand*
[2]*Department of Physics, Centre for Advanced Instrumentation, Durham University, South Road, Durham DH1 3LE, UK*
[3]*Science Faculty, Lampang Rajabhat University, Chomphu, Mueang, Lampang 52100, Thailand*

Accepted 2024 March 7. Received 2024 March 6; in original form 2023 November 23

ABSTRACT

This study utilized advanced numerical simulations with the Weather Research and Forecasting model coupled with Chemistry (WRF-Chem) to predict anticipated astronomical seeing conditions at the Thai National Observatory (TNO). The study evaluated the effects of both gas-phase and aerosol-phase chemical processes in the Earth's atmosphere, along with the impact of spatial and temporal resolution on model performance. These simulations were validated against measurements from the Differential Image Motion Monitor (DIMM) and the Slope Detection and Ranging (SLODAR) technique. Due to the inherent temporal variability of the DIMM observations, a 24-h moving average window was applied to both DIMM data and WRF-Chem model outputs. This reduced the percentage root-mean-square error in the comparison between the two data sets from 23 per cent to 11 per cent and increased the correlation coefficient from 0.21 to 0.59. Chemistry played a minor role during the study period, contributing 3.49 per cent to astronomical seeing. However, it did affect the model's accuracy. Additionally, the study revealed that higher spatial and temporal resolution simulations did not necessarily improve the model's accuracy. When compared to SLODAR observations of the refractive index structure constant (C_n^2dh), the simulations captured altitude variations within ±25 per cent above 5 km and 25–50 per cent below 5 km. Dome seeing also played a role, contributing to around 90 per cent or more in the lowest altitude layer. The results emphasized the significance of seeing predictions in providing valuable insights into complex atmospheric phenomena and how to mitigate the effects of atmospheric turbulence on telescopes.

Key words: turbulence – atmospheric effects – site testing – software: simulations.

1 INTRODUCTION

The Thai National Observatory (TNO), operated by the National Astronomical Research Institute of Thailand (NARIT), is a facility equipped with advanced astronomical instruments, including a 2.4-m telescope, a 0.7-m telescope, and several smaller instruments. Situated on the highest mountain in Thailand, Doi Inthanon, at an elevation of approximately 2.455 km above sea level, the selection of the TNO site took into account factors such as its geographic location, atmospheric conditions, and logistical considerations.

A crucial factor that affects astronomical observations is atmospheric turbulence, commonly known as 'seeing'. This phenomenon arises from the unpredictable motion of air in the Earth's atmosphere, distorting the light from celestial objects as it passes through. Seeing has a significant impact on the resolution and contrast of astronomical images, particularly in the visible and near-infrared wavelengths. To optimize observation strategies and instrument performance at the TNO, it is essential to comprehend the expected seeing conditions at the site.

This article presents the findings of simulations conducted at the TNO using an advanced numerical model. These simulations consider the unique meteorological and atmospheric conditions specific to the TNO site, allowing the prediction of the anticipated seeing conditions. The Weather Research and Forecasting model coupled with Chemistry (WRF-Chem) is a state-of-the-art numerical model known for its high precision in simulating meteorological and atmospheric conditions concerning both spatial and temporal resolution. WRF-Chem has proven successful in simulating various atmospheric phenomena, including air pollution, atmospheric chemistry, and climate change (Reddington et al. 2019; Bran et al. 2022). This article also evaluates the performance of WRF-Chem in predicting the meteorological and atmospheric conditions at the TNO site. The output of the model was utilized to simulate the expected seeing conditions under different observing conditions, providing valuable insights for optimizing observation and instrument configurations.

Numerous studies were undertaken to investigate simulations of astronomical seeing using the Weather Research and Forecasting

★ E-mail: ronmcdo@gmail.com (RM); timothy.butterley@durham.ac.uk (TB); thiranan.sonkaew@gmail.com (TS)

(WRF) model. Trinquet & Vernin (2007) conducted a statistical analysis of meteorological balloon profiles, identifying the lognormal distribution of temperature, buoyancy force, and wind speed shear fluctuations. Their resulting model estimated optical turbulence strength (C_n^2) based on macroscopic meteorological parameters, unveiling a new relationship for large-scale turbulence description. This model's capability to forecast optical turbulent layer strength and altitude was verified, enhancing the understanding and prediction of atmospheric conditions. Giordano et al. (2013) validated the WRF model alongside turbulence parametrization for forecasting atmospheric and optical conditions at the Observatorio del Roque de Los Muchachos (ORM) in La Palma, Canary Islands. By comparing forecasted WRF data with *in situ* measurements, they demonstrated agreement in meteorological parameters at ground level and nightly/monthly seeing forecasts. This underscored WRF's potential in optimizing observatory scheduling. Similarly, Giordano et al. (2014) employed WRF to identify optimal astronomy sites, particularly La Palma, Canary Islands. Utilizing the Trinquet–Vernin (TV) model, they analysed spatial forecasted conditions, introducing a quality parameter (Q) for site assessment. This study supported site selection and confirmed ORM' suitability. Liu et al. (2015) characterized atmospheric optical turbulence at the Large Sky Area Multi-Object Fiber Spectroscopic Telescope (LAMOST) site, comparing measurements with global observatories. They used WRF coupled with the TV model to estimate local optical turbulence parameters. Cuevas et al. (2018) simulated optical turbulence in Armazones and Paranal using combined refractive index structure constant models. They employed WRF to derive the vertical structure of C_n2 and astronomical seeing. Qian et al. (2021) modelled atmospheric turbulence at the Ali observatory in Tibet with WRF, showing agreement with radiosonde data. Rafalimanana et al. (2022) optimized ground-based observation scheduling with WRF's meteorological parameters integrated into an optical turbulence model. Yang et al. (2022) used Polar WRF to simulate astronomical seeing at Antarctica's Dome A, confirming its reliability for scheduling observations. Shikhovtsev et al. (2023) utilized WRF to describe atmospheric flow at the Baikal Astrophysical Observatory, uncovering mesoscale vortex structures affecting image quality and turbulence. They developed a turbulence model and optimized profiles, considering direct solar observations.

Several studies were also conducted using global circulation models and other mesoscale models. Osborne & Sarazin (2018) compared astro-meteorological parameters and Earth's atmospheric turbulence profile from a forecast model based on a general circulation model from the European Centre for Medium-Range Weather Forecasts and a turbulence profiling instrument (the stereo-Scintillation Detection and Ranging or stereo-SCIDAR). The model compared well with measurements, showing a high correlation of 0.98 for turbulence profiles and 0.64, 0.40, and 0.63 correlations for free atmosphere seeing, isoplanatic angle, and coherence time, respectively. This model's speed and accuracy could aid in scheduling optimal astronomical observations and enhancing adaptive optics (AO) systems. Masciadri, Turchi & Martelloni (2019, 2020) discussed recent advancements in implementing operational forecast systems for ground-based telescopes with AO and ground stations supporting free-space optical communication. The authors presented an improved version of their Advanced LBT (Large Binocular Telescope) Turbulence and Atmosphere (ALTA) forecast system, which utilizes numerical forecasts and real-time measurements to achieve highly accurate predictions of atmospheric and astroclimatic parameters on short time-scales. Additionally, they addressed differences and misconceptions in optical turbulence forecasting using mesoscale and general circulation models. In 2020, Masciadri et al. likewise applied a novel autoregressive technique to forecast optical turbulence at Paranal, building on the success of the ALTA Center's approach for LBT observations. This method, incorporating real-time measurements and mesoscale atmospheric modelling, achieved remarkable accuracy with a root-mean-square error (RMSE) of 0.1 arcsec for 1-h seeing forecasts and a high 98 per cent probability of detecting weak seeing conditions. The study also expanded this approach to other astroclimatic parameters beyond seeing. Masciadri, Turchi & Fini (2022) also emphasized the significance of short-term (1–2 h) forecasts for new-generation facilities like ELTs with AO, particularly for service mode operations. Using an autoregressive method combining mesoscale atmospheric models and real-time measurements, they achieved exceptional accuracy in predicting seeing and atmospheric parameters, outperforming both longer term forecasts and persistence-based methods. The approach, initially implemented for LBT observations, is extended to the Very Large Telescope site, covering various astroclimatic parameters, and is planned for operational use, showcasing improved accuracy compared to machine learning methods and persistence predictions.

Overall, these recent studies highlighted the continued importance of accurate astronomical seeing simulations for optimizing telescope performance and observing strategies. The use of numerical models such as WRF-Chem can provide valuable insights into the complex atmospheric phenomena that impact astronomical observations and can complement traditional meteorological measurements and observations. Future research could focus on further refining and validating these models for use at various astronomical sites, as well as developing new techniques for mitigating the effects of atmospheric turbulence on telescope performance.

Section 2 describes the forecasting system utilized, as well as the observations used in the validation. Section 3 discusses the comparison of the simulations with the observations, the effects of chemical and aerosol processes, the effects of spatial and temporal resolution, the comparison of the simulations to turbulence profiles, the spatiotemporal characteristics of the simulated atmospheric turbulence, and finally the operationalization of the system. Section 4 summarizes the study and suggests recommendations.

2 METHODOLOGY

Our seeing simulations are based on the TV model (Trinquet & Vernin 2007) and the study of Giordano et al. (2013) to calculate optical turbulence utilizing the WRF-Chem model (v.4.3.1) optimized for the mainland Southeast Asian region configured as in Bran et al. (2022), but using updated terrestrial data (Manomaiphiboon et al. 2017), the Mellor-Yamada Nakanishi and Niino (MYNN) Level 3 planetary boundary layer scheme (Olson et al. 2019), and updated anthropogenic emission inventories for northern Thailand (Jansakoo, Surapipith & Macatangay 2022) along with contributions from the Emission Database for Global Atmospheric Research collaboratively with the task force for Hemispheric Transport of Air Pollution (EDGAR-HTAP) (Janssens-Maenhout et al. 2015). This is an improved version of Macatangay & Rattanasoon (2021) which simply uses WRF (v.3.8.1) without chemistry coupling. WRF-Chem takes into account a wide range of atmospheric parameters, including temperature, pressure, humidity, wind speed, turbulence, and chemistry. Using this model, we simulated not only the atmospheric conditions at the TNO site for a range of observing conditions but also gas-phase and aerosol-phase chemical processes for air quality applications over the mainland Southeast Asian domain. This approach was taken since the astronomical observing season (November–May) coincided with the forest fire season (February–

April), which prompted the need to address air quality applications as well. The simulations were performed for a period of one observing season, from 2022 December to 2023 April. The model domain covered the entire mainland Southeast Asia, with a horizontal grid spacing of 9 km. Initial and boundary conditions were taken from the National Centers for Environmental Prediction (NCEP) and Global Data Assimilation System Final analysis (GDAS/FNL) 0.25 Degree Global Tropospheric Analyses and Forecast Grids (National Centers for Environmental Prediction/National Weather Service/NOAA/U.S. Department of Commerce 2015) for the meteorology, and the Whole Atmosphere Community Climate Model (WACCM) configuration of CESM2, for the chemistry (Gettelman et al. 2019). The Fire Inventory from NCAR (FINNv1.5) (Wiedinmyer et al. 2011) and the Model of Emission of Gases and Aerosols from Nature (MEGAN) (Guenther et al. 2006) were also utilized for fire and biogenic emissions, respectively.

The WRF-Chem model output was validated against meteorological data as well as aerosol concentration observations (Bran et al. 2022) since aerosols can affect atmospheric turbulence and therefore the astronomical seeing conditions. The WRF-Chem hourly output was used to simulate the expected seeing conditions and the refractive index structure constant (C_n^2) at the TNO site for different observing conditions and compared it with the existing Differential Image Motion Monitor (DIMM) and the Slope Detection and Ranging (SLODAR) measurement technique that has been installed at the site on a campaign basis.

The DIMM technique involves observing the motion and fluctuations of stellar images caused by the Earth's atmosphere. It utilizes a telescope to focus on a relatively bright star and records the changes in the star's image over a short period, typically a few milliseconds (Sarazin & Roddier 1990). By analysing the recorded images, the DIMM can determine the atmospheric turbulence's impact on the incoming light and quantify the seeing conditions. The primary parameter obtained from a DIMM observation is the seeing parameter, often represented as the full width at half-maximum (FWHM) of the stellar images. This parameter indicates the size of the point spread function of the star, which is affected by atmospheric blurring. A smaller FWHM value corresponds to better seeing conditions and higher image quality. DIMM measurements are valuable for astronomers and observatories to evaluate and compare different observing sites, assess the quality of astronomical conditions, and optimize the planning and execution of observations. It aids in selecting the most suitable locations for astronomical observatories and telescopes, where atmospheric turbulence is minimized to obtain clearer and more detailed astronomical images. Since DIMM seeing measurements have a lot of inherent temporal variability owing to its high temporal resolution (10 s in this study), boxplot analysis was employed to remove the outliers (termed as 'outlier-free DIMM'). An hourly moving average was also utilized to further smooth the DIMM seeing data (termed as 'hourly smoothed DIMM'). The impact of varying the moving average window (3, 6, 12, and 24 h) on the performance metrics of the model was also examined. This included evaluating the effects on both the DIMM outlier-free data and the WRF-Chem hourly output. The performance metrics considered were mean and standard deviation values (Stdev), RMSE, percentage RMSE (per cent RMSE), and correlation coefficient (R).

SLODAR is a method of measuring the strength of optical turbulence as a function of altitude above the observatory (Wilson 2002). It is an optical triangulation technique that utilizes a double Shack–Hartmann wavefront sensor to measure wavefront slopes from two stars simultaneously. The atmospheric turbulence profile (C_n^2) is recovered by fitting a model to the measured wavefront slope covariances (Butterley, Wilson & Sarazin 2006). Knowledge of the turbulence profile at an observatory site is important for the design of astronomical AO systems. AO systems make real-time adjustments to deformable mirrors or other optical components within telescopes, thereby compensating for atmospheric distortions and improving the quality of astronomical images. The TNO SLODAR instrument is deployed on the 2.4 m telescope and has a vertical resolution of approximately 2 km.

3 RESULTS AND DISCUSSION

This section discusses the comparison of the WRF-Chem astronomical seeing simulations with the observations in the following sequence: comparisons with DIMM observations (Section 3.1) with a focus on the effects of chemical and aerosol processes (Section 3.1.1), as well as the effects of spatial and temporal resolution (Section 3.1.2); the comparison of the simulations to turbulence profiles from SLODAR observations (Section 3.2); the spatiotemporal characteristics of the simulated atmospheric turbulence (Section 3.3), and finally the operationalization of the system (Section 3.4).

3.1 Simulation comparisons with DIMM measurements

Using boxplot analysis, DIMM seeing values above 2.18 arcsec (regarded as outliers) were removed to reduce the inherent temporal variability in the DIMM measurements (termed as 'outlier-free DIMM') due to the high temporal resolution of the raw data (10 s). 2022 December DIMM data were also excluded from the analysis since instrument testing was being performed during this period. This is shown in Fig. 1 (grey dots). Also shown are the hourly smoothed (1-h moving average) DIMM seeing data (red dots) as well as the WRF-Chem seeing simulations (blue line).

According to our simulations, the expected seeing conditions at the TNO during the study period exhibited an average value of 1.38 ± 0.11 arcsec, with an RMSE of 0.29 (23 per cent) arcsec when compared to the DIMM observations. The hourly smoothed DIMM observations themselves yielded a mean value of approximately 1.26 ± 0.20 arcsec during the study period. Given the inherent temporal variability of the DIMM observations, even after a 1-h moving average window was employed (red dots in Fig. 1), the nightly (approximately between 6 PM and 6 AM local time when DIMM measurements were available) averaged astronomical seeing was calculated for the DIMM observations as shown in Fig. 2. Likewise, the nightly averaged astronomical seeing for the WRF-Chem simulations was also computed (Fig. 2). The correlation coefficient (R) between the two data sets was then calculated to be 0.21.

The application of moving average windows of 3, 6, 12, and 24 h to both the DIMM observations and the WRF-Chem model outputs resulted in enhancements in RMSE, per cent RMSE, and R values, as outlined in Table 1. The best model performance metrics were produced by the 24-h moving average window. The time series for the 24-h moving average window is depicted in Fig. 3. In this specific analysis, the 24-h moving average window produced the optimal balance between smoothing the data (noise reduction) and capturing significant trends. Applying the 24-h moving average window reduced short-term fluctuations, unveiling important trends while avoiding excessive smoothing. A too-narrow window misses these aspects.

The differences observed between the WRF-Chem simulations and DIMM observations can be potentially influenced by several factors. These include limitations inherent to the model itself, the

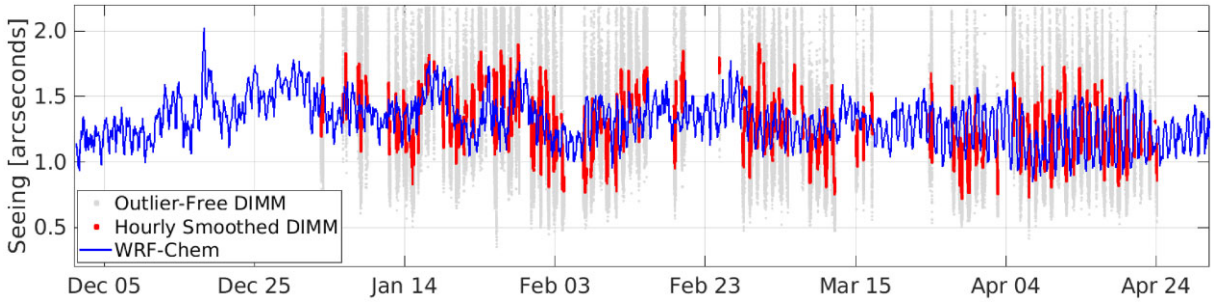

Figure 1 Comparison of the astronomical seeing at the TNO in northern Thailand from DIMM measurements and from WRF-Chem simulations from 2022 December 1 to 2023 April 30. Shown are the outlier-free DIMM seeing measurements (grey dots) from 2023 January 1 to 2023 April 30 (2022 December DIMM data were excluded due to instrument testing), hourly smoothed DIMM seeing data (red dots) and WRF-Chem seeing simulation outputs (blue line).

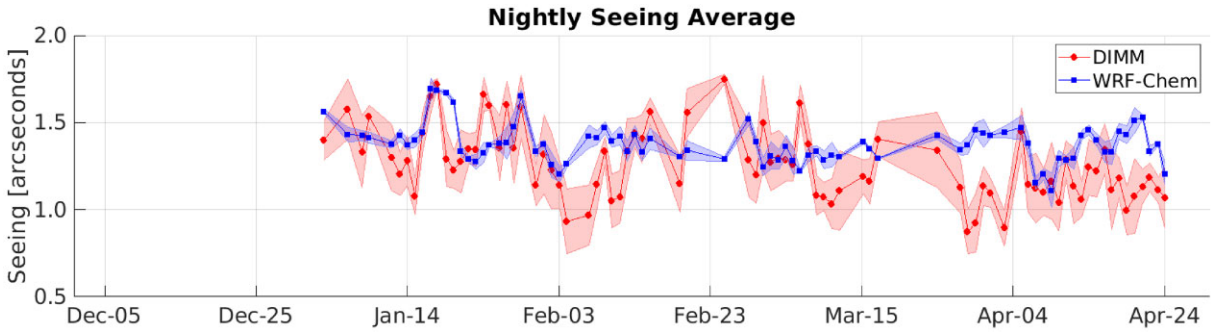

Figure 2 Nightly seeing averages of the hourly smoothed DIMM data (red dots with red line) and the WRF-Chem hourly model outputs (blue dots with blue line). The shaded areas indicate 1σ standard deviations of the nightly averages.

Table 1 Effect of increasing the moving average window for the DIMM observations and smoothing the WRF-Chem model outputs on the model performance metrics.

Moving average window [h^{-1}]	Mean seeing (WRF-Chem)[arcsec]	Stdev (WRF-Chem)[arcsec]	Mean seeing (DIMM)[arcsec]	Stdev (DIMM)[arcsec]	RMSE [arc-sec]	Per cent RMSE [per cent]	Nightly averaged R
1	1.38	0.11	1.26	0.20	0.29	23	0.21
3	1.38	0.11	1.27	0.18	0.25	20	0.23
6	1.37	0.11	1.26	0.17	0.22	18	0.30
12	1.35	0.11	1.27	0.16	0.19	15	0.40
24	1.30	0.11	1.26	0.15	0.13	11	0.59

quality of input data, the spatial and temporal resolution of the simulations, and limitations specific to the DIMM instrument.

Regarding the model limitations, WRF-Chem is a numerical weather prediction model that incorporates aerosol physical and chemical processes, aerosol-gas chemistry, and its meteorological interactions. However, it relies on assumptions and parametrizations that may not precisely represent real-world conditions (Baklanov et al. 2014; Sokhi et al. 2022). The accuracy of WRF-Chem simulations depends on the quality of the input data used, such as initial conditions and boundary conditions for chemical and meteorology, and emissions inventories. Incomplete or erroneous input data can contribute to discrepancies with observations obtained from the DIMM instrument, affecting the fidelity of the simulated astronomical seeing.

Furthermore, the spatial and temporal resolution of the WRF-Chem simulations is limited by the finite grid it operates on. This resolution may not capture small-scale atmospheric features or localized effects accurately, unlike the DIMM observations, which directly measure atmospheric turbulence and provide high-resolution information. Simulations of meteorological and chemical parameters could be significantly influenced by topographic effects (Bran et al. 2022), especially over mountainous regions. Such disparities can result in differences between the model's predictions, including the simulated astronomical seeing, and the actual observations.

Furthermore, while DIMM observations provide valuable insights into atmospheric seeing, they are not without limitations. These limitations encompass various factors such as instrumental noise, calibration errors, dome seeing, and the prevailing atmospheric conditions during observations (Bally et al. 1996; Aristidi et al. 2019). Recent assessments comparing the accuracy of different instruments, particularly with respect to Stereo-SCIDAR (Scintillation Detection and Ranging), reveal a notable challenge: it appears unattainable to measure the seeing with an accuracy within 0.2 arcsec across diverse instruments (Osborn et al. 2018). Furthermore, Masciardi, Lombardi & Lascaux (2014), performed a comprehensive comparison of Multi-Aperture Scintillation Sensor (MASS) and Generalized-SCIDAR

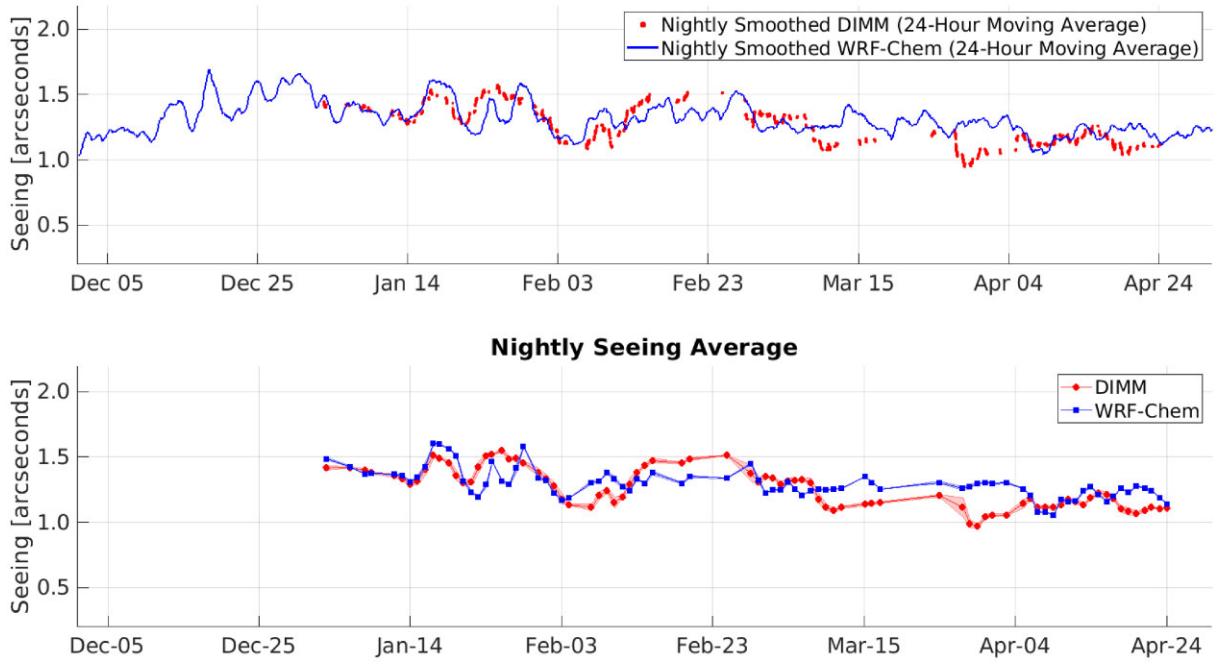

Figure 3 Applying a 24-h moving average window to both DIMM observations and WRF-Chem model outputs (top panel). Nightly seeing averages of the 24-h smoothed data (bottom panel).

instruments, vital for measuring optical turbulence distribution, using DIMM measurements for cross-validation, aiming to assess measurement reliability and understand their limitations in characterizing turbulence stratification in the atmosphere, ultimately concluding the need for cautious interpretation and potential risk associated with their usage. This discrepancy underscores the complexities inherent in accurately characterizing atmospheric turbulence and its impact on astronomical observations. Therefore, while DIMM remains a valuable tool, its interpretations should be approached with caution, considering the intrinsic limitations and potential disparities in measurement accuracy among different instrumentation methodologies. These factors can introduce uncertainties or biases when comparing the results of the model with the DIMM observations, thereby impacting the assessment of the simulated astronomical seeing.

3.1.1 Effect of chemical and aerosol processes

Regarding the effect of chemical and aerosol processes, a detailed analysis was conducted by re-simulating the entire study period without chemistry. This allowed us to investigate the contribution of chemical and aerosol processes to the simulated astronomical seeing.

The results of the re-simulations indicated that chemistry only contributed 3.49 per cent to the simulated astronomical seeing at the study site (TNO) during the entire study period. However, chemistry did have an impact on the model performance as shown in Table 2.

It is important to recognize that the role of chemistry and aerosol processes can vary depending on factors such as atmospheric conditions, geographical location, and period. In certain regions or during particular time frames, the role of chemistry in shaping atmospheric conditions and aerosol distribution can be more pronounced. As a result, when examining the simulated astronomical seeing, it is crucial to assess the contribution of chemistry within the specific conditions and context of the study.

3.1.2 Effect of spatial and temporal resolution

Re-simulations were conducted to investigate the impact of spatial resolution. Multiple nested domains with spatial resolutions of 9, 3, and 1 km were utilized, and they interacted with each other in what we term 'multidomain (with feedback)'. These simulations were carried out solely from 2023 January 20 to February 1, without incorporating chemistry due to limitations in our current computational resources and storage capacity. This specific time frame was selected as it offered the highest number of DIMM observations for validation purposes. Additionally, another re-simulation was performed with 1-min model outputs at a spatial resolution of 1 km. The outcomes of these re-simulations are presented in Table 3.

It can be noted that higher spatial and temporal resolution simulations do not necessarily improve model performance. Several potential factors could explain this outcome. Running simulations with higher spatial and temporal resolution over complex terrain could highly affect the dynamics of microphysics, which reflect in wind shear, airmass advection, and convection, specifically with the feedback mechanism in multiple nested domains. Additionally, such simulations require more computational resources and longer computational times and can therefore be more prone to numerical instabilities, which can degrade the accuracy of the simulation and produce higher RMSE.

When analysing the effects of temporal resolution on the simulation results, a higher temporal output frequency of 1 min at 1 km spatial resolution resulted in increased variability in the output, with the average hourly values aligning with the results obtained from the 1 km hourly output simulation. It is important to note that running simulations with higher temporal resolution requires significantly more computational resources and time compared to the 9 km hourly output configuration, making it impractical for operational forecasting given our current computational limitations.

Higher temporal resolution simulations also generate a significantly larger amount of data compared to coarser temporal res-

Table 2 RMSE between simulations and DIMM observations during the entire study period with and without the effect of chemical and aerosol processes.

With/without chemistry	Spatial resolution [km]	Temporal resolution output	Mean RMSE [arcsec]
With chemistry	9	hourly	0.29
Without chemistry	9	hourly	0.30

Table 3. RMSE between simulations and DIMM observations during the period from 2023 Jan 20–Feb 1, at different spatial and temporal resolutions.

With/without chemistry	Single/multi domain (with feedback)	Spatial resolution [km]	Temporal resolution output	RMSE [arcsec]
With chemistry	single domain	9	hourly	0.26
Without chemistry	single domain	9	hourly	0.26
Without chemistry	multidomain (with feedback)	9	hourly	0.27
Without chemistry	multidomain (with feedback)	3	hourly	0.30
Without chemistry	multidomain (with feedback)	1	hourly	0.31
Without chemistry	multidomain (with feedback)	1	1-min	0.30

olutions. Storing and processing this extensive data set can pose challenges, especially when dealing with limited storage capacities and analysis capabilities.

In summary, the analysis of the effect of chemistry and spatial resolution on the simulated astronomical seeing revealed that, for the specific study period and location, chemistry only had a minor contribution, but had an effect on model performance. However, the importance of chemistry and aerosol processes can vary, and their significance should be assessed within the context of the study's specific conditions. Regarding spatial and temporal resolution, higher resolutions may introduce complexities that can affect the model's performance, and careful consideration of model physics, parametrizations, initialization, boundary conditions, and computational resources is necessary to achieve more accurate simulations.

3.2 Simulation comparisons with SLODAR measurements

Simulated profiles (using the 9 km spatial resolution, single domain, and chemistry configuration) of the altitude-weighted refractive index structure constant, C_n^2dh, were also compared with SLODAR observations as shown in Fig. 4. The model generally captured the C_n^2dh above approximately 5 km (maximum of approximately $\pm$25 per cent difference). However, there is a significant model and observation difference below approximately 5 km (from 25 per cent to 50 per cent difference). There could be several reasons for the significant difference between the model and observation of the refractive index structure constant, C_n^2dh, below approximately 5 km. Below 5 km, the atmosphere can exhibit complex and localized phenomena, such as boundary layer turbulence, low-level jets, or atmospheric waves. These phenomena may not be fully captured or parametrized accurately in the model, resulting in discrepancies with the observations. The model might also not include all the relevant physical processes that contribute to the generation and dissipation of turbulence in the lower atmosphere. For instance, processes like convective turbulence or gravity waves could have a significant impact on C_n^2dh. Modelling of the boundary layer is still a challenge (Holtslag et al. 2013).

The SLODAR observations themselves may have uncertainties or limitations that affect the accuracy of the measured C_n^2dh profiles. Instrumental errors, atmospheric conditions during the observations, or other factors could introduce biases or noise in the data, making it difficult to directly compare with the model (Butterley et al. 2006). The lower atmosphere is highly variable in both space and time. Small-scale variations in atmospheric conditions or short-term fluctuations in turbulence levels could also contribute to the observed differences. Dome-seeing can also have an effect. Since the simulations do not include the dome, the influence of turbulence inside the dome can also be estimated. Approximately 97.4 per cent, 89.8 per cent, and 89.7 per cent of the bottom-most layer come from the dome seeing for the observations of 2022 December 17, 2023 February 13, and 2023 April 14, respectively.

A detailed statistical analysis of the comparison of SLODAR observations and WRF-Chem model outputs of C_n^2dh is shown in Table 4. The average per cent magnitude of the differences between the predicted values and the actual values is given by the per cent RMSE. In this context, lower per cent RMSE values indicate better predictive accuracy, as they represent smaller errors between predictions and actual data.

The 95 per cent confidence interval for the per cent RMSE provides a range of values within which we can reasonably expect the true per cent RMSE to lie 95 per cent of the time if the same experiment or analysis were to be repeated multiple times. This interval reflects the uncertainty associated with the per cent RMSE estimation based on the available data. This means that the calculated per cent RMSE falls within the range of values that are statistically plausible given the uncertainty in the data and analysis. The wider the confidence interval, the more uncertainty there is about the true per cent RMSE value. A smaller RMSE and a narrower confidence interval are generally desirable, as they indicate better predictive accuracy and higher confidence in the results.

The per cent RMSE and the widths of confidence intervals between the SLODAR observations and the WRF-Chem model outputs increased from 2022 December to 2023 February and to 2023 April measurements. This indicates increased variability in the turbulence observations as recorded by SLODAR that the model could not capture well. Further explanation is provided in the next section.

3.3 Simulated altitude-refractive index structure constant (C_n^2dh)-time series

The altitude-refractive index structure constant (C_n^2dh) time series provides valuable information about the spatio-temporal characteris-

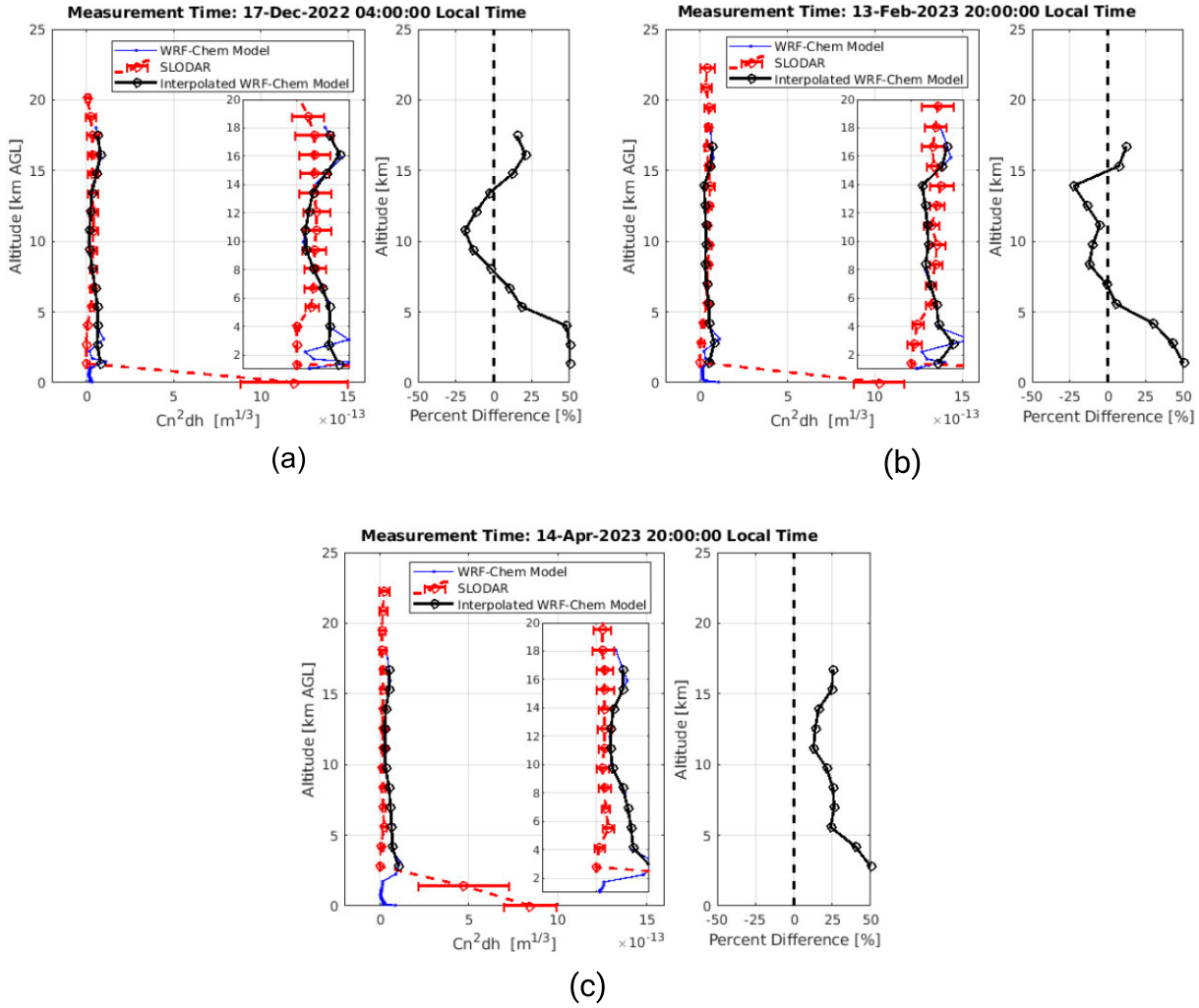

Figure 4 SLODAR measurements of C_n^2dh as compared with the WRF-Chem model for 2022 December 17 (a), 2023 February 13 (b), and 2023 April 14 (c). Also shown are insets from 1 to 20 km to exclude the bottom-most and top-most layers, as well as the per cent difference altitude profiles.

Table 4 Statistical metrics on the comparison of SLODAR observations and WRF-Chem model outputs of C_n^2dh.

Statistical metrics	SLODAR measurement dates		
	2022 Dec 17	*2023 Feb 13*	*2023 Apr 14*
RMS $[m^{\frac{1}{3}}]$	3.90×10^{-14}	3.29×10^{-14}	4.54×10^{-14}
Per cent RMSE [per cent]	53.3	47.0	63.7
Lower confidence interval [per cent]*	34.7	27.2	38.3
Upper confidence interval [per cent]*	69.3	64.9	91.6
Confidence interval width [per cent]*	34.6	37.7	53.3
Per cent dome seeing	97.4	89.8	89.7

Note. *95 per cent confidence interval

tics of atmospheric turbulence and is crucial for various applications in atmospheric sciences, astronomy, and optical communications. Since the SLODAR observations were only performed at specific periods due to measurement limitations, the validated simulated time-series profiles of C_n^2dh can give a general description of the turbulence over TNO with an altitude range limited by the model domain, which is from the ground up to around 18 km. This is depicted in Fig. 5 a few days before and after the SLODAR measurements on 2022 December 17, 2023 February 13, and 2023 April 14.

A consistent relatively strong refractive index structure constant (C_n^2dh) value can be seen from the simulations between around 2–

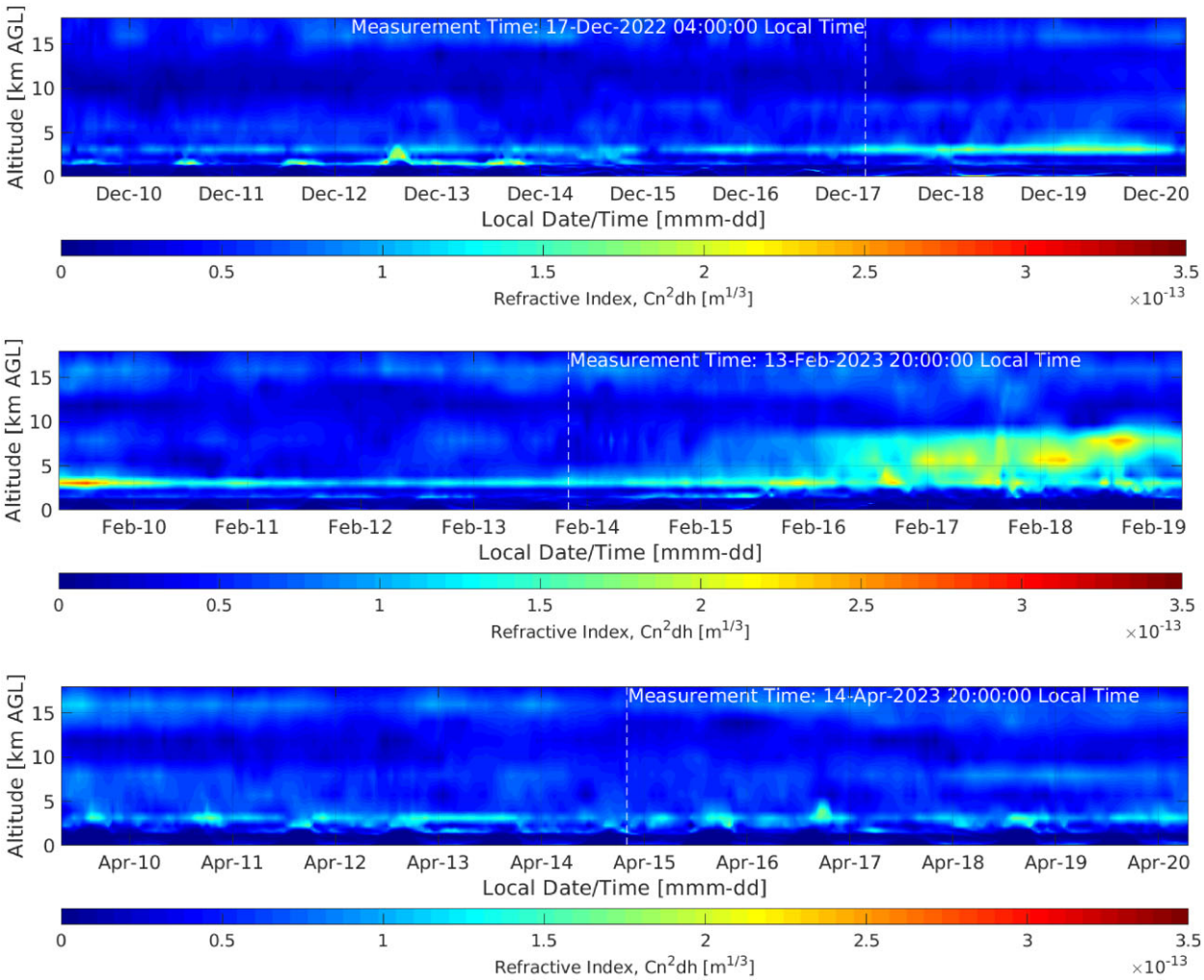

Figure 5 Daytime and nighttime C_n^2dh profiles during SLODAR measurements (dotted white line) on 2022 December 17 (top panel), 2023 February 13 (middle panel), and 2023 April 14 (bottom panel).

4 km over the TNO in Doi Inthanon, Thailand (Fig. 5). This can be attributed to several atmospheric factors. The first is orographic effects. Doi Inthanon is a mountainous region, and the presence of mountains can significantly impact local atmospheric conditions. As air flows over the mountains, it can generate turbulence and vertical mixing, leading to increased C_n^2dh values at certain altitudes, including around 4 km. Secondly, convective instability. Diurnal heating and cooling cycles can create convective currents and thermal gradients, resulting in atmospheric instability. This instability can lead to the development of turbulence and elevated C_n^2dh values. Thirdly, local weather patterns. Weather systems, such as thunderstorms or frontal activity, can introduce significant variations in atmospheric conditions. These systems can generate turbulence and increase C_n^2dh values, particularly at specific altitudes. This is evident after the SLODAR measurements on 2023 February 13 (middle panel of Fig. 5) during around 2023 February 16, and after when very strong refractive index structure constants were seen ranging up to around 2–10 km. During this period, severe thunderstorms occurred over the region. Fourthly, effects from the atmospheric boundary layer. The boundary layer, which is influenced by the characteristics of the underlying surface, can play a role in turbulence generation. The stability or instability of the boundary layer can impact C_n^2dh values at different altitudes. Fifth, seasonal variations. The C_n^2dh values and variabilities can vary throughout the year due to changes in atmospheric conditions associated with different seasons. Over the study site and during SLODAR observations, December is the cool dry season, February is the transition period towards the warm dry season, and April is the transition period towards the wet season.

3.4 Operationalization

A website to display both DIMM observations and simulated forecasts of astronomical seeing together with selected meteorological parameters has been developed and is currently under testing and evaluation by astronomers using the facility. It can be accessed under the address http://weather.narit.or.th/tno_observer, but active only during the observing season (November–May). A screenshot of the test website is shown in Fig. 6. The website can serve as a guide for astronomers employing TNO in their research to assess their observation strategies and the weather in general. For the operational runs of the WRF-Chem (v. 4.3.1) forecast model, the 9 km spatial resolution, single domain, 6-d forecast, and with chemistry configuration using the Global Forecasting System for the meteorological boundary conditions (NCEP, 2007) was employed due to a balance between accuracy and efficiency using our current computational resources and storage. The inclusion of chemistry

Figure 6 Screenshot of the test website showing the seeing and meteorological observations overlaid with the forecasts. It can be accessed through http://weather.narit.or.th/tno_observer during the observing season (November–May).

in the configuration, despite its minimal effect on astronomical seeing, is due to the anticipation of air quality applications alongside astronomical ones within the atmospheric forecasting system. A test website is also being developed and evaluated for this purpose (https://ronmcdo4.wixsite.com/atmos-predict) in combination with a data platform that is currently being developed.

4 CONCLUSION AND RECOMMENDATIONS

In conclusion, the article presented the results of simulations conducted at the TNO in Doi Inthanon, Chiang Mai, in northern Thailand. These simulations utilized the WRF-Chem to account for the specific meteorological and atmospheric conditions at the TNO site. The findings offer valuable insights into enhancing observation conditions and instrument configurations. Comparisons between the WRF-Chem simulations and DIMM measurements of seeing conditions at TNO revealed differences influenced by multiple factors, such as model limitations, data quality, simulation resolution, and the temporal variability of the DIMM instrument. Nevertheless, the simulations still provide useful information about the expected astronomical seeing conditions at the TNO site. The study also investigated the impact of chemical and aerosol processes on simulated astronomical seeing, indicating a minor contribution from chemistry during the study period, although it does affect the accuracy of the model. Furthermore, the study examined the effect of spatial and temporal resolution on model performance, demonstrating that higher resolution simulations do not necessarily improve accuracy. The use of numerical models like WRF-Chem can provide valuable insights into the complex atmospheric phenomena that affect astronomical observations. However, further research is necessary to refine and validate these models for use at different astronomical sites and to develop techniques to mitigate the effects of atmospheric turbulence on telescope performance. In summary, the article inferred the importance of precise astronomical seeing simulations in optimizing telescope performance and observing strategies.

ACKNOWLEDGEMENTS

The authors would like to thank the following: Jongkol Thiplird, Pinida Niyomprainiwet, Amonrat Wongarsa, Weeranuch Uadkla, Chakriya Sirirat, Aunchan Santipong, Thitaya Leartdamnern, Sorawit Somjit, Pattaravadee Jantawong, Thanyaluk Siwasopa, Anurak Chakpor, Jirasak Noisapung, Pathompong Butpan, Rungrit Anutarawiramkul, Pakawat Prasit, Vichawan Sakulsupich and Utane Sawangwit. This study is funded by the Thailand Science Research and Innovation under the project no. 180548.

DATA AVAILABILITY

The data underlying this article will be shared on reasonable request to the corresponding author.

REFERENCES

Aristidi E. et al., 2019, MNRAS, 486, 915
Baklanov A. et al., 2014, Atmos. Chem. Phys., 14, 317
Bally J. et al., 1996, Publ. Astron. Soc. Aust., 13, 22
Bran S. H., Macatangay R., Surapipith V., Chotamonsak C., Chantara S., Han Z., Li J., 2022, Atmos. Res., 277, 106303
Butterley T., Wilson R. W., Sarazin M., 2006, MNRAS, 369, 835
Cuevas O., Curé M., Escárate P., 2018, in Marshall H. K., Spyromilio J., eds, Proc. SPIE Conf. Ser. Vol. 10700, Ground-based and Airborne Telescopes VII. SPIE, Bellingham, p. 1070055
Gettelman A. et al., 2019, J. Geophys. Res.: Atmos., 124, 12380
Giordano C., Vernin J., Trinquet H., Muñoz-Tuñón C., 2014, MNRAS, 440, 1964
Giordano C., Vernin J., Vázquez Ramió H., Muñoz-Tuñón C., Varela A. M., Trinquet H., 2013, MNRAS, 430, 3102
Guenther A. et al., 2006, Atmos. Chem. Phys., 6, 3181

Holtslag A. A. M. et al., 2013, B. Am. Meteorol. Soc., 94, 1691
Jansakoo T., Surapipith V., Macatangay R., 2022, EnvironmentAsia, 15, 26
Janssens-Maenhout G. et al., 2015, Atmos. Chem. Phys., 15, 11411
Liu L.-Y., Giordano C., Yao Y.-Q., Vernin J., Chadid M., Wang H.-S., Yin J., Wang Y.-P., 2015, MNRAS, 451, 3299
Macatangay R., Rattanasoon S., 2021, J. Phys.: Conf. Ser., 2145, 012015
Manomaiphiboon K., Boonya-Aroonnet. S., Sarinnapakorn K., Assareh N., Aman N., Tantianuparp P., Thodsan T., Pratumthong A., 2017, Final Report, Hydro and Agro Informatics Institute
Masciadri E., Lombardi G., Lascaux F., 2014, MNRAS, 438, 983
Masciadri E., Turchi A., Fini L., 2022, in Schreiber L., Schmidt D., Vernet E., eds, Proc. SPIE Conf. Ser. Vol. 12185, Adaptive Optics Systems VIII. SPIE, Bellingham, 121851Q
Masciadri E., Turchi A., Martelloni G., 2019, preprint (arXiv:1911.02819)
Masciadri E., Turchi A., Martelloni G., 2020, in Schreiber L., Schmidt D., Vernet E., eds, Proc. SPIE Conf. Ser. Vol. 11448, Adaptive Optics Systems VII. SPIE, Bellingham, p. 114481I
National Centers for Environmental Prediction/National Weather Service/NOAA/U.S. Department of Commerce, 2015, updated daily. NCEP GDAS/FNL 0.25 Degree Global Tropospheric Analyses and Forecast Grids. Research Data Archive at the National Center for Atmospheric Research, Computational and Information Systems Laboratory. Available at: https://doi.org/10.5065/D65Q4T4Z
Olson J. B., Kenyon J. S., Angevine W. A., Brown J. M., Pagowski M., Sušelj K., 2019, A Description of the MYNN-EDMF Scheme and the Coupling to Other Componentsin WRF–ARW. NOAA Technical Memorandum OAR GSD-61, Boulder, Colorado
Osborn J. et al., 2018, MNRAS, 478, 825
Osborn J., Sarazin M., 2018, MNRAS, 480, 1278
Qian X., Yao Y., Zou L., Wang H., Yin J., Li Y., 2021, MNRAS, 505, 582
Rafalimanana A., Giordano C., Ziad A., Aristidi E., 2022, PASP, 134, 055002
Reddington C. L., Conibear L., Knote C., Silver B. J., Li Y. J., Chan C. K., Arnold S. R., Spracklen D. V., 2019, Atmos. Chem. Phys., 19, 11887
Sarazin M., Roddier F., 1990, A&A, 227, 294
Shikhovtsev A. Y. et al., 2023, Appl. Sci., 13, 6354
Sokhi R. S. et al., 2022, Atmos. Chem. Phys., 22, 4615
Trinquet H., Vernin J., 2007, Environ. Fluid Mech., 7, 397
Wiedinmyer C. et al., 2011, Geosci. Model Dev., 4, 625
Wilson R. W., 2002, MNRAS, 337, 103
Yang Q., Wu X., Wang Z., Hu X., Guo Y., Qing C., 2022, MNRAS, 515, 1788

This paper has been typeset from a TEX/LATEX file prepared by the author.